DIAL–phoswich hybrid system for remote sensing of radioactive plumes in order to evaluate external dose rate

ARTICLE *in* PROGRESS IN NUCLEAR ENERGY · APRIL 2009

Impact Factor: 1.12 · DOI: 10.1016/j.pnucene.2008.09.008

2 AUTHORS:

Gholamreza Shayeganrad
Università di Pisa
17 PUBLICATIONS **45** CITATIONS
SEE PROFILE

Parviz Parvin
Amirkabir University of Technology
164 PUBLICATIONS **617** CITATIONS
SEE PROFILE

Progress in Nuclear Energy 51 (2009) 420–433

Contents lists available at ScienceDirect

Progress in Nuclear Energy

journal homepage: www.elsevier.com/locate/pnucene

DIAL–phoswich hybrid system for remote sensing of radioactive plumes in order to evaluate external dose rate

Gholamreza Shayeganrad, Parviz Parvin*

Department of Physics, Amirkabir University of Technology, P.O. Box 15875-4413, Tehran, Iran

Keywords:
UV/visible DIAL
Phoswich detector
X/γ coincidence detection
Remote sensing
External dose rate
Uranium

A B S T R A C T

Radioactive pollutants which are released into the atmosphere are known to present a hazard to human health; therefore they must be identified and well protected. Here, an improved remote sensing system is investigated for monitoring radioactive plumes released into the atmosphere from nuclear sites. It is based on the combination of DIAL technique with a phoswich detector array. The DIAL, using a tunable UV/Vis laser, measures the concentration of the radionuclide and the plume distance, whereas the phoswich detects characteristic hard X/γ ray emissions. Here, we have shown the ability of a hybrid system for the prompt identification and quantification of the effluents containing the uranium radionuclide, using the parameters of uranium such as absorption cross-section, absorption spectrum and density.

1. Introduction

Environmental concerns about nuclear power plants are prompted mainly by the effects of the radiations on the population living in the neighborhood. Nuclear risk in any geographical area is connected with the nuclear sites, i.e. milling and mining facilities, fuel fabrication factories, reactor stacks or nuclear fuel reprocessing plants, in many areas. The Chernobyl core meltdown accident showed that the scale of impact can be very large and the risk of remote nuclear sites should also be of considerable concern for the area. Thus, it is important to obtain the geographic distribution of the nuclear risk based on the external dose.

Nuclear power plants usually release various gaseous and liquid effluents as well as highly radioactive mixture of fission products components in structural and cladding materials due to neutron activation as well as small amounts of long-lived transuranium elements ($Z > 92$) during their normal operation. The radionuclides discharge to atmosphere is evaluated to be ~1 TBq/GW (Lamarsh, 1983; Glasstone and Sesonske, 1994; United Nations Scientific Committee on the Effects of Atomic Radiation, 1988). However, all nuclear reactor systems are designed with a number of barriers that limit the escape of those radionuclides during normal operation and in the event of an abnormal occurrence. Table 1 gives the atomic and nuclear characteristics of the major radionuclides released from typical reactors and reprocessing plants to the environment in the routine operation and which of them are X/γ emitters (Kaeri; National Institute of Technology). In both pressurized-water reactors (PWR) and boiling-water reactors (BWR), the condenser steam-jet air ejectors and the turbine gland-seal system are two important sources that release gaseous radioactive products to the atmosphere through the stack. The individual dose is determined to be 0.2 μSv/yr, which is less than 0.1% of the background level radiation. They may emanate considerably more radioactivity higher than background level during the course of an accident, where especially radioactive gases are first released into the containment building and may leak to the atmosphere subsequently (Lamarsh, 1983; Glasstone and Sesonske, 1994). One should calculate the doses to public from such releases in order to evaluate the environmental impact of the operating plant to assure that this is within the acceptable standards.

Moreover, mining operations involve the removal of large quantities of ore containing uranium and its daughter products from the ground. It is several thousand times greater than the concentration of these nuclides in the rest of the natural terrestrial environment. It is well known that particulates in airborne dust which contain ^{238}U and its daughters and some times ^{232}Th and its daughters are hazardous to human health. Release from mining and milling facilities as well as effluents from fuel fabrication sites are estimated to be ~0.01–0.1 ppb. Comparably, the abundance of uranium in the earth crust is ~3–4 ppm, while ~1 ppb can be found in the human body (United Nations Scientific Committee on the Effects of Atomic Radiation, 1988). Table 2 illustrates the nuclear and atomic characteristics of the uranium chain elements of which most are alpha emitters possessing UV/Vis absorption lines

* Corresponding author.
E-mail address: parvin@aut.ac.ir (P. Parvin).

0149-1970/$ – see front matter © 2008 Elsevier Ltd. All rights reserved.
doi:10.1016/j.pnucene.2008.09.008

Table 1
Atomic and nuclear characteristics of the major radionuclide released from a typical reactor or a reprocessing plant.

Nuclide	Half-life	X- or γ-ray energies (keV) (Kaeri)	Strong absorption line (nm) (National Institute of Technology)	Recommended tunable lasers
^{86}Rb	18.631 d	1077.0	780.027	Ti:Al_2O_3 fundamental
^{89}Sr	50.53 d	908.7	460.733	Ti:Al_2O_3 SHG, Coumarine
^{91}Y	0.18 y	1204.8	407.7359	Ti:Al_2O_3 SHG, Coumarine
^{95}Zr	64.02 d	235.7, 724.2	383.5962	Ti:Al_2O_3 SHG
^{102}Rh	207 d	556.6	369.236	Ti:Al_2O_3 SHG
^{111}Ag	7.45 d	96.8, 245.4, 342.1	328.0680	Ti:Al_2O_3 THG
^{115}Cd	44.6 d	105.2, 158.0, 336.2	228.8022	Coumarine SHG, Ti:Al_2O_3 THG
^{125}Sn	8.04 d	270.6, 332.1	286.3315	Ti:Al_2O_3 THG
^{127}Sb	3.85 d	61.1, 252.4, 290.8	231.1463	Coumarine SHG, Ti:Al_2O_3 THG
^{137}Cs	30.04 y	283.5, 661.6	852.113	Ti:Al_2O_3 fundamental
^{140}Ba	12.752 d	30.0, 162.7, 304.9	553.5481	Ti:Al_2O_3 SHG
^{144}Ce	284.9 d	41.0, 80.1, 133.5	463.2320	Ti:Al_2O_3 SHG, Coumarine
^{147}Nd	10.98 d	91.1, 120.4, 275.4	463.424	Ti:Al_2O_3 SHG
^{151}Sm	90 y	21.5	436.2912	Coumarine fundamental
^{155}Eu	4.7611 y	45.3, 60.0, 86.5	459.403	Ti:Al_2O_3 SHG, Coumarine fundamental

(Kaeri; National Institute of Technology). Radionuclide decay processes often leave the product nuclide in an excited energy state. The product nuclide in such an excited state either falls directly to the ground state or in steps to lower energy states through the emission of energy as gamma or characteristic X-ray radiation. Fig. 1 shows the typical decay schemes of ^{226}Ra and ^{238}U. The excited nucleus ^{222}Ra usually falls to the ground state by emitting a hard X-ray of about 186 keV. Similarly, the excited ^{234}Th decays with accompanying the emission of two subsequent X-ray photons of 49.5 and 113.5 keV.

In addition, there is always a small amount of background radiation in the atmosphere present from cosmic and natural sources. A major natural source of radionuclides is radon, a noble gas product of radium decay. Radon may enter to the atmosphere as either of two isotopes, ^{222}Rn ($t_{1/2} = 3.8$ d) and ^{220}Rn ($t_{1/2} = 54.5$ s). Both emit alpha particles in decay chains that terminate with stable isotopes of lead as shown in Fig. 2.

The radioactivity from the ground is strongly varying, dependent on the living places. The radioactivity originates from long-lived isotopes with lifetime of order 10^9 years, particularly for ^{232}Th, ^{235}U and ^{238}U. Predominant gaseous effluent from active uranium mine is ^{222}Rn in the ventilation from underground mine or released into the pits from surface mine. Release rate of radon per unit mass of ore were estimated to be ~1 GBq/ton in underground mine and about 0.1 GBq/ton from surface mine while natural radon density is reported to be of ~7 Bq/m^3 (10^{-7} ppm). In general, the average human being from those natural sources receives a dose equivalent of approximately 2 mSv/yr (United Nations Scientific Committee on the Effects of Atomic Radiation, 1988).

Furthermore, cosmic rays act on nuclei in the atmosphere to produce other radionuclides, including ^{3}H, ^{7}Be, ^{10}Be, ^{14}C, ^{22}Na, ^{32}P, ^{39}Cl, and ^{33}P. The cosmic radiation from the space, including the radiation from the sun, consists mainly the highly energetic protons, alpha particles and to some extent of heavier charge particles to give a dose of about 10 μSv/y on the ground level (United Nations Scientific Committee on the Effects of Atomic Radiation, 1988).

Before the practice was discontinued, the above ground detonation of nuclear weapons added large amounts of radioactive particulate matter to the atmosphere as well. Because of food contamination and biouptake, the most serious fission contaminant products from this source were ^{90}Sr, ^{131}I, and ^{137}Cs. The two latter isotopes are absorbed by human organs to establish the major sources of the internal dose.

Generally, the radionuclide pollutants are known to be hazardous for human health, therefore they must be quickly identified and well protected, mainly by the continuous environmental monitoring equipments which includes surveillance and checking relevant to assessing the behavior and pathways of radionuclides for environmental safety particularly at nuclear facilities. Remote sensing of radioactive elements are desired to answer which source appears to be the most dangerous for people living close to the nuclear sites and which regions are at the highest risks from an accidental release.

To our knowledge, there are few works available on the remote measurement of radioactive species. One approach that provides a unique signature is nuclear quadrupole resonance (Garroway et al., 2001). The other methods are based on secondary radioactive effects including anomalous gaseous fields and their emission in optical and microwave range and passive registration of the optical fluorescence emission of highly ionized air induced by α, γ and X radiations. Those methods are characterized by low signal to noise ratio because of a large amount of atmospheric natural and artificial sources radiation appears within the spectral range (Chistrykova and Kopytin, 2005).

On the other hand, a known technique for remote sensing of X/γ emitter species within the plume released into the atmosphere is the X/γ spectroscopy, using large scintillator crystals for surveying the scintillator efficiency, based on the detection of photopeak energies and the relative amplitudes (Parvin et al., 2004, 2005;

Table 2
Atomic and nuclear characteristics of some uranium chain and transuranium elements from mining and milling facilities or fuel fabrication plant.

Nuclide	Principle decay mode	Half-life	X- or γ-ray energies (keV) (Kaeri)	Strong absorption line (nm) (National Institute of Technology)	Recommended tunable lasers
^{238}U	Alpha	4.56×10^9 y	49.55, 1	351.4610	Ti:Al_2O_3 SHG, XeF
^{234}Pa	Beta	6.75 h	131.3, 99.9	398.223	Ti:Al_2O_3 SHG
^{230}Th	Alpha	8.0×10^4 y	49.5, 113.5	371.94347	Ti:Al_2O_3 SHG
^{226}Ra	Alpha	1.62×10^3 y	186.2	482.591	Ti:Al_2O_3 SHG
^{210}Po	Alpha	138.4 d	803.1	248.008	Ti:Al_2O_3 THG
^{206}Pb	Stable	–	–	283.3053	Ti:Al_2O_3 THG

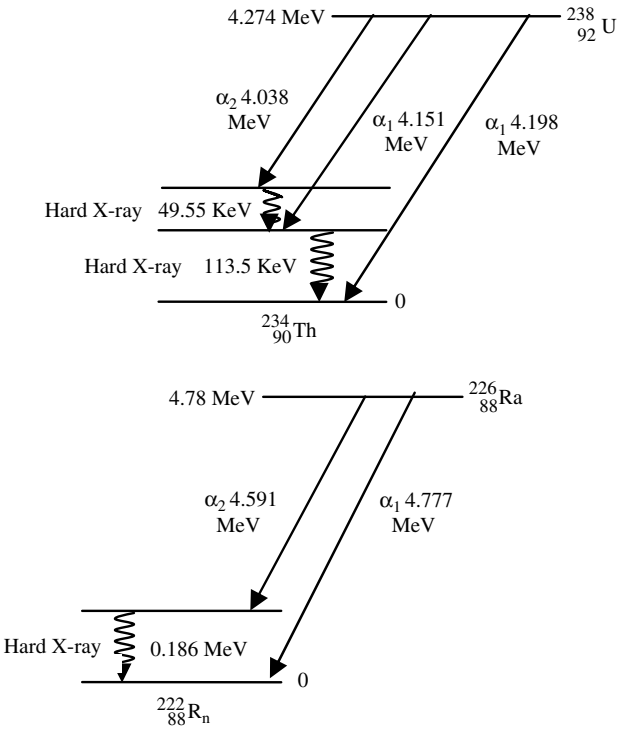

Fig. 1. Typical α-decay schemes of $^{238}_{92}$U and $^{228}_{88}$Ra.

Parvin and Davoudabadi, 2007; Knoll, 2000). Generally, scintillation counters are very common and yield a very high efficiency above 30 keV, while large scintillators increase the background noise.

In order to reduce the background noise, it is well known to exploit a couple of dissimilar scintillators with different decay time constants, so called phoswich (Phosphor Sandwich) (Parvin and Davoudabadi, 2007; Parvin et al., 2005; Knoll, 2000). It offers fast response, lowest detection limits and better precision analysis of the coincidence signals by employing the pulse shape analyzer (PSA) and the pulse shape discriminator (PSD). It measures characteristic X or γ photopeaks of radioactive elements to identify the constituents as well as their relative concentrations even in the presence of high level background radiation. However, phoswich by itself is unable to evaluate the external dose rate. It does not determine the absolute concentration of the radionuclide element within the plume to discern a far plume with high activity from a weak one nearby.

On the other hand, measurements using optical spectroscopic methods are well known to provide remote sensing with the unique advantages such as extremely high sensitivity, fast response and molecular or atomic selectivity. A number of the passive remote sensing techniques for detecting, identifying and quantifying signature of the plumes are the hyper spectral infrared spectroscopy and Echell grating spectrometer. Various techniques of laser spectroscopy which have been successfully employed in atmospheric and environmental research are laser induced fluorescence (LIF), photoacoustic detection, spontaneous Raman scattering, coherent anti-Stokes Raman spectroscopy, laser induced breakdown spectroscopy (LIBS) and differential absorption lidar (DIAL) (Svanberg, 2001; Demtröder, 2003; Weitkamp, 2005; Fujii and Fukuahi, 2005).

Among those instruments, UV/Vis-DIAL offers unique advantages for radioactive element detection mainly because of strong atomic absorption cross-section (10^{-11}–10^{-12} cm^2) at that spectral range. It is a most successful technique which omits the laser excess noise caused by spectral interference. A number of UV/Vis laser remote sensing instruments operate for meteorological and measuring atmospheric optical parameters of ozone, water vapor, aerosols and clouds. Those include UV high spectral resolution tunable lidar, fourth and third harmonic Ti:Al_2O_3, SHG/THG tunable dye laser in UV range as well as single frequency triplet Nd:YAG laser and various excimer lasers (Svanberg, 2001; Demtröder, 2003; Weitkamp, 2005; Fujii and Fukuahi, 2005; Camagani and Sandroni, 1984; Uchino, 2006; Kildal and Byer, 1971; Guerra et al., 1994; Fredriksson et al., 1979; Kobayashi et al., 2004; Edner et al., 1987; Beniston et al., 1990). Presently, remote sensing of toxic chemical and aerosol pollutants using various tunable UV lasers are being extensively investigated. UV-DIAL is actually used to measure the continuous concentration of atmospheric trace of SO_2 and O_3 conveniently due to the emission from smoke stacks or volcanoes (Fugii et al., 2001; Egeback et al., 1984). The DIAL technique is also used for the determination of the stratospheric ozone profile. An XeCl excimer laser is used to tune the strong ozone absorption line while a third harmonic Nd:YAG laser is employed as a reference wavelengths (Derava et al., 2004). Also, lidars using resonance fluorescence can be used in the range from 75 to 117 km, where suitable constituents such as Na, K and Fe with large scattering cross-section exist to produce strong resonance fluorescence signals. Although, the backscatter cross-sections of fluorescence is approximately 10^{14} times higher than Rayleigh backscattering cross-sections, conversely, because of quenching in the lower atmosphere due to high density of the atoms, molecules and aerosols, the fluorescence technique is not suitable. Indeed, the application of fluorescence lidar is limited for remote sensing because of detector sensitivity coupled with solar background radiation.

Here the DIAL–phoswich hybrid system is introduced, which is potentially an advantageous technique to investigate the dynamic effluent parameters of a radioactive plume such as uranium. It consists of both passive nuclear and active atomic detection units. It is based on a phoswich detector array to trace species due to their characteristic hard X- and γ-ray emissions accompanying a differential absorption lidar coupled with a tunable UV/Vis laser. It is mainly useful for rapid identification of the unknown radioactive elements within the plume as well as the corresponding concentration, the exact location and external dose rate. We have shown that the application of the combined technique noticeably enhances the system efficiency.

Indeed, the hybrid system is proposed here in order to act as a novel technique for the remote sensing of the radioactive plume,

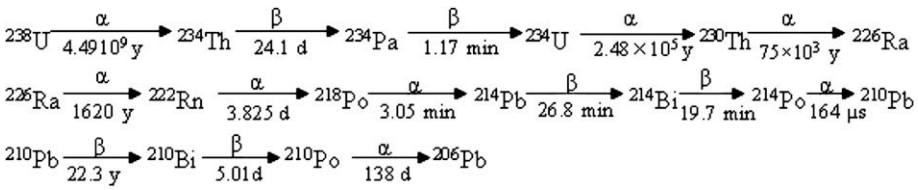

Fig. 2. Decay chain of uranium.

as to an efficient instrument for element tracing, uranium mine exploration and the health physics applications. Consequently, the spacecraft equipped with the hybrid system enables the scientists to explore the radioactive sources in the solar system, such that a portable hybrid instrument mounted on a rover makes Mars mission more attractive.

2. Apparatus

The hybrid system includes a transmitter, a receiver, phoswich scintillators coupled with photomultiplier tubes (PMTs) array, pulse shape analyzer (PSA), anticoincidence unit, multichannel analyzer (MCA) and the data processor equipped with interactive software for real time control and data acquisition with the access to atomic and nuclear data libraries. The transmitter employs the pulsed tunable UV/Vis laser and the receiver consists of a Cassegrain telescope, a Lyot tunable birefringent filter or a Fabry-Perot interference filter and a PMT detector. PMT is generally used as a low noise and sensitive detector for UV and visible spectral region. It offers fast response and high gain as well as good quantum efficiency.

2.1. Phoswich detector array (PDA)

A phoswich detector is a combination of two dissimilar scintillators optically coupled to a single PMT, employing pulse shape analyzer (PSA) to suppress background in the counting X-ray. It consists of a typical thin NaI(Tl) and a thick CsI(Tl) within different decay times, 0.25 μs and 1 μs, respectively, so that, the shape of the output pulse from the PMT is dependent on the relative contribution of scintillation light from the two scintillators. The NaI(Tl) and CsI(Tl) crystals are designed to be ~3 and ~20 mm thick. Lightly penetrating radiations in spectral range ~30–300 keV, are stopped fully in the first scintillator, but more penetrating MeV photons may generate light in the thick one. PSA and PSD unites identify the signals due to each scintillator. Those distinguish that the energy deposition in which scintillator occurs. The events generating light in both scintillators are denied to suppress the noise for X-ray counting.

When an X-ray photon from the source enters the detector through a mechanical collimator, it will generally interact with an iodine atom in the NaI crystal. This interaction occurs at a single point in the crystal and causes an electron to be ejected from the atom. This electron then excites the light-generating modes of the crystal to create scintillation in the form of a pulse of light, whose intensity is proportional to the energy of the original X-ray, to be viewed through a PMT. This tube converts the pulse of light into an amplified electrical charge signal. Thus, the amplifier and the subsequent electronics deal with a peak voltage of the pulse that is proportional to the initial X-ray energy. By calibrating the exact relation between incident X-ray energy loss and the digitized value of the voltage pulse height, the inferred incident energy of the X-ray is revealed. Alternatively, separate electronic pulses are derived from the fast and slow components of the PM tube signals.

Fig. 3 shows the performance of a typical PDA, including about 80 standard phoswich detectors each one having ~100 cm^2 area subtended together to constitute an array of 1 m diameter with the same area of telescope in DIAL unit. PSA unit discriminates between NaI events (left) and CsI events (right) using an MCA. Events resulting in scintillations from both volumes can be recognized by their pulse shape and can thus be rejected for X-ray detection, whereas those scintillate simply in CsI are accepted to detect γ photons. Phoswich resolution at 100 keV, 1 MeV and 662 keV are, respectively, about 5–7%, 5% and 6–7% (Frontera et al., 1997; Reddy and Ramamorthy, 2000; Farsoni and Hamby, 2007). The electronics using PSA is capable of discriminating events in 30–300 keV X-ray energies and up to several MeV gamma photons. It is characterized by a couple of peaks, one due to NaI(Tl) and the other due to CsI(Tl) events. The scale in abscissa is correlated with the decay time of the scintillation pulses. The selection of X-ray events is performed through PSD unit using the choice of lower and upper thresholds in the electronic unit.

When the source is assumed to be small in comparison to the distance, it is treated as a point source to emit X/γ photons isotropically. Hence, at a distance R from the source, the photons are distributed uniformly over a sphere of area $4\pi R^2$. Those are attenuated by the factor $\exp(-\mu R)$ traveling through the air, where μ is the total attenuation coefficient in air which is dependent on the photon energy. Therefore, the X/γ-ray intensity received by a detector located at distance R from the plume, is given by (Lamarsh, 1983; Glasstone and Sesonske, 1994):

$$I = \frac{C\exp(-\mu R)}{4\pi R^2} \text{ photons/m}^2\text{ s} \quad (1)$$

where C denotes the activity of the interest species in Bq. Consequently, the count M read by phoswich array can be written as:

$$M = \frac{\eta A T_{\text{int}} C\exp(-\mu R)}{4\pi R^2} \quad (2)$$

where η, A and T_{int} are the detector efficiency, the detector area and the integration time, respectively.

Phoswich is inherently a low noise limited detector, typically 100 counts/m^2 s at sea level. Apparently, this figure also takes into account the background radiation coming from the surrounding of the detector. The critical limit of detection, L_C, is defined to be $L_C = 2.33\sigma$, where 2.33 is known as the protection factor and σ denoted standard deviation (Chistrykova and Kopytin, 2005). If total counts of detector exceed L_C, then it is assumed that some real activity of the source is available. Moreover, for the total count smaller than L_C, it is concluded that the plume does not contain any significant activity. As the radioactive decay is a random process with a Poisson distribution; therefore the standard deviation is $\sigma = \sqrt{M}$, where M denotes the number of counts for a given integration time. As a consequent, any counting rate larger than 100 Hz/m^2 can be ascribed to be a signal such that

$$L_C = 23.3\sqrt{AT_{\text{int}}} \quad (3)$$

By equating Eqs. (2) and (3), the minimum detectable activity of the plume by phoswich, C_{md}, is obtained as

$$C_{\text{md}} = \frac{93.2\pi R^2 \exp(\mu R)}{\eta\sqrt{AT_{\text{int}}}} \quad (4)$$

The characteristic parameter of phoswich, $\eta C_{\text{md}}\sqrt{AT_{\text{int}}}$, versus plume distance, R, is depicted in Fig. 4 for several values of X or γ energies. It indicates that C_{md} decreases at higher X/γ energies for a definite plume distance. Similarly, C_{md} increases at longer distances for a definite X/γ energy. Moreover, the value is reduced for closer or larger source at longer integration time or greater area of the array detector. Typically, for the 150 keV X photons, a detector with $\eta = 100\%$ and $A = 1$ m^2 located at 100 m far from the plume during an integration time of 100 s, using Eq. (4), C_{md} is calculated to be equivalent to 45 μCi.

Fig. 5 plots phoswich counts in terms of the plume distance for a definite activity at various energies based on Eq. (2). In fact, phoswich does not function as a perfect remote sensor; because it is unable to discern a far dense plume from a near field dilute one. Moreover, at a definite plume distance, phoswich cannot differentiate whether plume contains high activity at smaller γ energy or low activity at higher γ energies. For example, 100 keV with 10^7 Bq or 10 MeV with 10^3 Bq are shown identical counting at 550 m. It

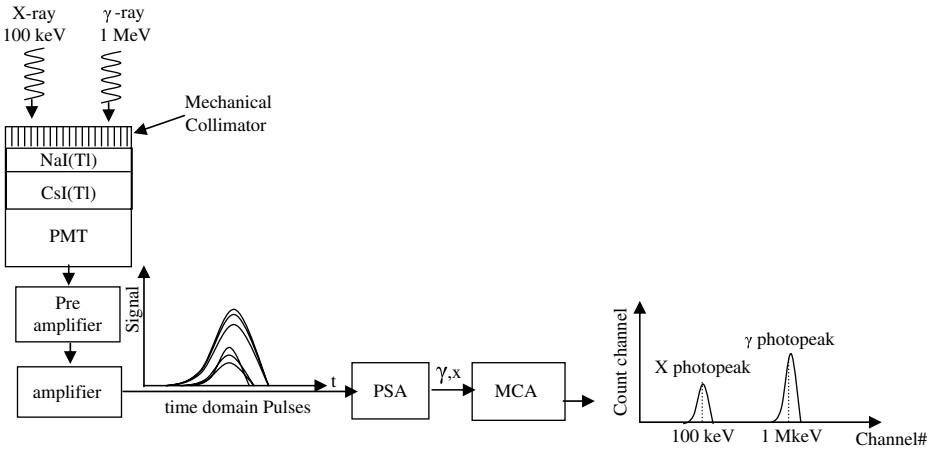

Fig. 3. Performance of phoswich dual energy analyzer.

arises from the fact that greater atmospheric attenuation takes place at higher gamma energies. Consequently, as its major disadvantage, phoswich by itself is unable to determine the external dose.

2.2. Differential absorption lidar (DIAL)

High sensitivity with good spatial resolution for long-range dynamic monitoring of the plume constituents can be achieved by the combination of differential absorption and scattering. DIAL includes high degree of sensitivity per probe energy and the capability of wavelength scanning over a wide variety of molecules and atoms having absorption characteristic in the spectral range as well as the quantitative evaluation of desired species. A typical DIAL system often sends a pair of pulsed laser wavelengths into the atmosphere. Those are close to each other with a large absorption coefficient difference, one at the tuned line, λ_{on}, where the species under investigation absorb and the other at a nonabsorbing detuned line, λ_{off}. A couple of such wavelengths, rather than a single one, are needed in order to strongly reduce the effect of the extinction in the atmosphere, mostly due to the scattering, and to correct the instrument calibration constant. When laser wavelength is much greater than the scatter size which is valid for the gaseous plumes, the Rayleigh scattering occurs with the backscatter cross-section proportional to λ^{-4}. Conversely, for water drops, clusters, dust, volcanic ashes, smokes or the aerosols under the condition that the scatter size is being greater than laser wavelength, the Mie scattering becomes dominant. The corresponding cross-section is more complex than Rayleigh scattering with wavelength dependence proportional to λ^{-x} where $0.4 < x < 0.5$.

The backscattered light from a range R is collected by the optical telescope mounted adjacent to the laser in a time delay $(2R/c)$, where c is light velocity. The power from a range interval $\Delta R = (c\tau_l/2)$ at range R is given by the general lidar equation as below (Weitkamp, 2005; Fujii and Fukuahi, 2005):

$$P_s(\lambda,R) = P_0 \frac{A}{R^2}\xi(\lambda)\beta(\lambda,R)\xi(R)\left(\frac{c\tau_l}{2}\right)\exp\left(-2\int_0^R \alpha(\lambda,R)\,dR\right) \quad (5)$$

where P_s is instantaneous power received by the detector from the range R. P_0, τ_l, β, α and A are the transmitted power, pulse duration, volume backscattering coefficient, extinction coefficient and telescope area, respectively. $\xi(\lambda)$ and $\xi(R)$ are defined to be the spectral gain coefficient of the receiver and the geometrical factor of the telescope, respectively. Usually β and α consist of contribution from both air molecules and aerosols. For altitudes below 100 km, an

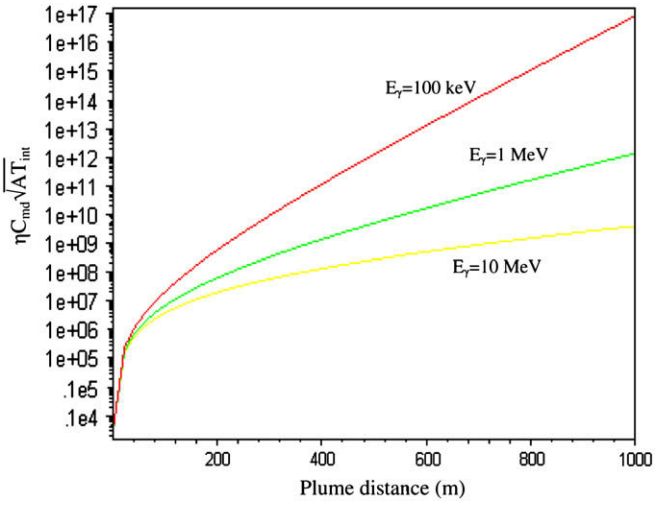

Fig. 4. Phoswich characteristic parameter $\eta C_{dm}\sqrt{AT_{int}}$ versus plume distance for various X/γ photon energies.

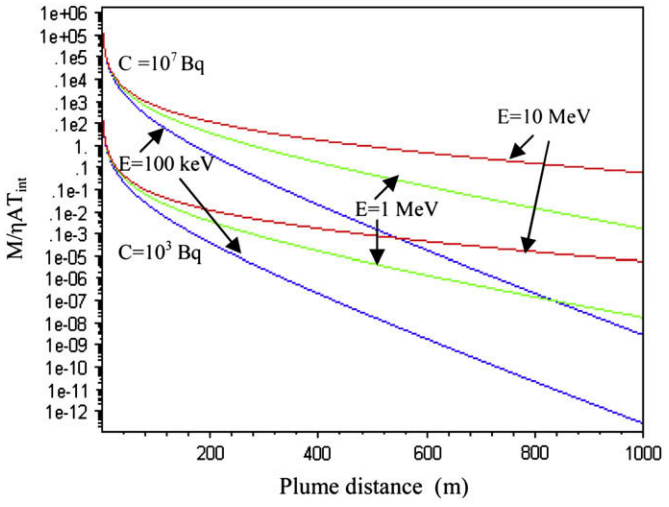

Fig. 5. Phoswich normalized counts, $M/\eta AT_{int}$, versus plume distance for various plume activities and different gamma energies.

approximate expression for the molecular backscatter coefficient, β_M, is written as below (Vaughan, 2002)

$$\beta_M(\lambda) = (\lambda_0/\lambda)^{4.09}\exp(-R/R_0)\times 10^{-7}\ \ m^{-1}sr^{-1} \quad (6)$$

where $\lambda_0 = 1.064\ \mu m$ and $R_0 = 8$ km. For $R \ll R_0$, the dependence β_M on the distance is negligible. Thus it is simplified to

$$\beta_M(\lambda) \approx (\lambda_0/\lambda)^{4.09}\times 10^{-7}\ \ m^{-1}sr^{-1} \quad (7)$$

For $\lambda = 351.46107$ and 591.5385 nm, β_M is found to be $\approx 9\times 10^{-6}$ m^{-1} sr^{-1} and $\approx 10^{-6}$ m^{-1} sr^{-1}, respectively, whereas the experimental data shows that the aerosol backscatter coefficient, β_A, denotes $\approx 10^{-7}$ $m^{-1}sr^{-1}$ at $2.09\ \mu m$. The altitude dependence is strong, reducing to a background level of nearly $3\times 10^{-10}\ m^{-1}\ sr^{-1}$ (Hannon et al., 1997).

The total attenuation factor, $\alpha(\lambda,R)$, can be written as:

$$\alpha(\lambda,R) = \alpha_{atm}(\lambda,R) + N(R)\sigma_{abs}(\lambda) \quad (8)$$

where, $\alpha_{atm}(\lambda,R)$ represents the atmospheric attenuation coefficient, $N(R)$ is the number density of the radionuclide species in the plume and $\sigma_{abs}(\lambda)$ represents the species absorption cross-section at λ.

By dividing the received power at λ_{on} over that of λ_{off} based on Eq. (5), the species concentration, $N(R)$, can be derived as:

$$N(R) = \frac{1}{2\Delta\sigma}\frac{d}{dR}\left(\ln\frac{P_s(\lambda_{off},R)}{P_s(\lambda_{on},R)}\right) - \frac{1}{2\Delta\sigma}\frac{d}{dR}\left(\ln\frac{\beta(\lambda_{off},R)}{\beta(\lambda_{on},R)}\right) - \frac{1}{\Delta\sigma}\left[\alpha_{atm}(\lambda_{off},R) - \alpha_{atm}(\lambda_{on},R)\right] \quad (9)$$

This equation is known as the DIAL equation. Here $\Delta\sigma = \sigma_{abs}(\lambda_{on}) - \sigma_{abs}(\lambda_{off})$ is the differential absorption cross-section of the species of interest.

Before a DIAL system is designed, the differential absorption of the target species must be known, in order to derive the necessary parameters such as laser energy, linewidth, and detector area. Also, the sensitivity and lower detection limit of the DIAL measurement is directly dependent on the accuracy of the differential absorption cross-section. In practice, the absorption lines in the visible and near UV can be measured accurately in the laboratory, and can generally be transposed to the atmospheric conditions afterwards.

On the other hand, an expression with good approximation for the peak value of the atomic absorption cross-section at center wavelength λ_{12} associated with the transition between ground state $|1\rangle$ and the upper state $|2\rangle$ is given by (Drake, 2006; Axner et al., 2004)

$$\sigma_{12} = \sigma_{ref}\frac{4}{\gamma_e}\left(\frac{g_2}{g_1}\right)\left(\frac{\lambda_{ref}}{\lambda_{12}}\right)|\langle 1|\vec{r}|2\rangle|^2$$

or

$$\sigma_{12} = \sigma_{ref}\frac{4}{\gamma_e}\left(\frac{g_2}{g_1}\right)\left(\frac{\lambda_{12}}{\lambda_{ref}}\right)^2\left(\frac{A_{21}}{A_{ref}}\right) \quad (10)$$

where $\sigma_{ref} = 0.1523\times 10^{-6}\ m^2\ s^{-1}$, $A_{ref} = 0.1367\times 10^8\ s^{-1}$, $\lambda_{ref} = 529.177$ nm, $\langle 1|\vec{r}|2\rangle$, λ_{12}, A_{21}, g_1 and g_2 are reference of cross-section, A-factor and wavelength, dimensionless electrical dipole moment, absorption wavelength, A-factor of the transition and degeneracy of the states $|1\rangle$ and $|2\rangle$, respectively, and γ_e denotes the sum of the all emission rates ($\Sigma_i A_{2i}$) such that for a collisionally dominated medium takes a value of ~ 1 GHz (Axner et al., 2004).

For a number of the species of interest, the spectral properties in UV/Vis region is summarized in Table 3. As seen, the atomic absorption cross-section is in order of 10^{-11}–10^{-12} cm^2 which is much larger than those of the molecules ($\sim 10^{-17}$–10^{-21} cm^2). It leads to a higher detection sensitivity and SNR for the atomic species remote sensing.

The last expression in the right hand side of Eq. (9) is known as systematic error. Since the absorption lines of the most atmosphere constituents, such as O_3, SO_2 and NO_2 lie in UV/Vis region, the systematic error increases mainly due to different extinction and backscatter properties of the atmosphere at the DIAL probe wavelengths. Among the expected noise (or interference) from those species in the atmosphere, O_3 is considered as the dominant constituent. The ozone density in normal dry air is reported to be $\sim$0.01–0.04 ppm (Vesilind et al., 1988), which increases up to $\sim$0.04–0.08 ppm after beginning sunshine, large enough to be compared to the typical stratospheric ozone peak of $\sim$0.06 ppm (Nakazato et al., 2006). Fig. 6 shows the ozone absorption spectrum having a band continuum in the UV (200–350 nm with a peak at $\sim$255 nm) and the visible (400–700 nm with a peak at $\sim$600 nm) spectral region (Molina and Molina, 1986). Consequently, systematic error is given by:

$$T_{O_3}(R) = \frac{\Delta\alpha_{atm}}{\Delta\sigma} = \frac{\Delta\sigma_{O_3}}{\Delta\sigma}N_{O_3}(R) \quad (11)$$

where $\Delta\alpha_{atm}$ is the differential extinction coefficient of the atmosphere,$N_{O_3}(R)$ represents the concentration of ozone gas with a differential absorption cross-section $\Delta\sigma_{O_3}$. In the atomic remote sensing, T_{O_3} lies in the interval of $\sim 10^3$–10^7 cm^{-3}. It is estimated to be $\sim 10^3\ cm^{-3}$ in remote sensing of uranium element at $\lambda_{on} = 351.46107$ nm and $\lambda_{off} = 352.26107$ nm. Therefore, we can neglect the noise caused by ozone compared to the uranium concentration above stacks of the nuclear site which is reported to be $\sim$0.01–0.1 ppb ($\sim 10^8$–$10^9\ cm^{-3}$) (United Nations Scientific Committee on the Effects of Atomic Radiation, 1988). In addition, the probe lines λ_{on} and λ_{off} are close together such that their difference is slightly greater that Doppler-limited linewidth ($\lambda_{off} = \lambda_{on} \pm 2\delta\lambda_D$), where $\delta\lambda_D \approx 0.75$ pm. By definition, λ_{off} lies in the tail of absorption spectrum and λ_{on} represents the peak. Those lines exhibit the same scattering properties according to Eq. (8). Hence, Eq. (9) is simplified to

$$N(R) = \frac{1}{2\Delta\sigma}\frac{d}{dR}\left(\ln\frac{P_s(\lambda_{off},R)}{P_s(\lambda_{on},R)}\right) \quad (12)$$

It indicates that $N(R)$ is proportional to the logarithmic derivative of the backscattered signal ratio. The large Mie scattering cross-section of aerosols and dust in the path of the laser beam provides a strong signal at both wavelengths, to localize the plume accordingly. In gaseous plume, the backscattering peak due to Rayleigh scattering at λ_{off} is negligible. A drastic drop at location of the gaseous plume due to the strong absorption at λ_{on} is proportional to the species concentration. The break point predicts the location of the effluent diffusing into the atmosphere.

PMT is often used in UV/Vis-DIAL system as an efficient detector. They offer fast response and higher gain coupled with fairly good quantum efficiency and relatively low noise level. There are two main noise components: (i) dark current due to thermal emission and shot (or statistical) noise and (ii) noises including A/D conversion and that due to the signal amplification. In practice, there are other sources that also contribute to the shot noise of a PMT. One important source is the photons from the background radiation which scattered from the lower atmosphere and impinges on the detector.

Fig. 7 shows the background spectral radiance distribution of the cloudless sky (Partt, 1969). The distribution from the sun is enhanced towards the blue region because of the strong wavelength dependence of Rayleigh scattering. Furthermore, there is

Table 3
Some of transition properties of several radioactive elements.

Element	Absorption lines (nm) (National Institute of Technology)	A_{ki} (10^8 s^{-1}) (National Institute of Technology)	Relative intensity	g_1	g_2	Cross-section (10^{-12} cm^2)
Rb	420.180	0.018	11	2	4	1.01
	421.553	0.018	6	2	2	0.50
	780.027	0.370	1000	2	4	71.65
	794.760	0.340	500	2	2	34.18
Sr	460.733	2.01	1000	1	3	203.7
	689.253	0.00048	20	1	3	0.109
Y	407.7359	1.1	900	4	4	29.10
	414.2841	1.6	800	4	4	43.70
Rh	339.682	0.65	400	10	10	11.94
	350.252	0.43	600	10	10	8.40
	369.236	0.91	1000	10	8	15.80
Ag	328.0680	1.47	1000	2	4	50.36
	338.2887	1.35	500	2	2	24.59
Cd	228.8022	5.3	800	1	3	132.47
Sn	224.6057	1.48	300	1	3	35.65
	286.3315	0.544	700	1	3	21.29
Sb	206.8344	1.81	400	4	6	18.48
	217.5818	1.75	600	4	4	13.18
	231.1463	1.69	1000	4	2	7.18
I	178.276	2.71	150	4	4	13.70
	183.038	0.16	1000	4	6	1.28
Cs	455.528	0.0188	15	2	4	1.24
	459.317	0.0080	8	2	2	0.268
	852.113	0.3276	1000	2	4	75.71
	894.347	0.287	1000	2	2	36.53
Ba	307.1584	0.41	30	1	3	18.47
	350.1108	0.35	80	1	3	20.48
	553.5481	1.19	1000	1	3	174.09
Nd	463.424	0.84	1000	9	7	22.33
	468.345	0.52	600	9	9	18.15
	471.902	0.33	500	9	9	11.70
	492.453	0.90	900	9	11	42.45
	495.478	0.29	600	9	11	13.85
Sm	436.2912	0.49	300	1	3	24.73
Eu	311.1427	0.34	90	8	10	6.55
	321.2804	0.33	90	8	8	5.42
	333.4313	0.39	90	8	6	5.18
	459.403	1.60	1000	8	10	53.74
	462.722	1.53	900	8	8	52.13
	466.188	1.45	800	8	6	37.61
U	348.93672	0.13	500	13	11	2.13
	351.46107	0.12	500	13	15	2.72
	356.18038	0.057	400	13	11	0.97
	358.48774	0.19	1000	13	15	4.48
	381.19911	0.16	600	13	13	3.70
	387.10353	0.19	500	13	13	4.53
	394.38161	0.21	400	13	13	5.20
	415.39710	0.12	300	13	15	3.80
	436.20510	0.11	130	13	15	3.84
	591.5385	0.045	70	13	15	2.89

a general ~300 K radiation in the IR region due to the thermal emission of the atmosphere. At wavelength shorter than ~320 nm, the intensity of sunlight penetrating the atmosphere is reduced due to absorption of ozone and the O_2.

As illustrated in Tables 1 and 2, most of the absorption lines of radionuclides are in the regions with the strong solar background. So that eliminating the background radiation during daytime should be taken into account. The contribution of this noise source can be minimized by using a narrow bandwidth interference filter at the desired laser wavelength.

According to Fig. 7, assuming a diffraction-limited telescope with 1 m diameter, the background photons rate from the cloudless daytime sky is ~50000 counts per second (cps) at 351.46107 nm using a narrowband filter ~1 nm. The transmission bandwidth reduces to ~2–4 pm by situation a properly designed stack of Fabry-Perot filter as a second stage (McKay, 1999). It leads to a reduction of the background count by approximately two orders of magnitude, resulting in 100–200 cps. It is noticeable to mention that dark count rate of PMT depends on the cathode type, as well as the cathode area and the temperature. It is 30–80 cps at −25 °C and 2000 cps at 25 °C. Consequently, the background noise is suppressed by the implementation of appropriate filter.

Signal to noise ratio (SNR) is the significant parameter in the signal-detection discipline to resolve true signal from the

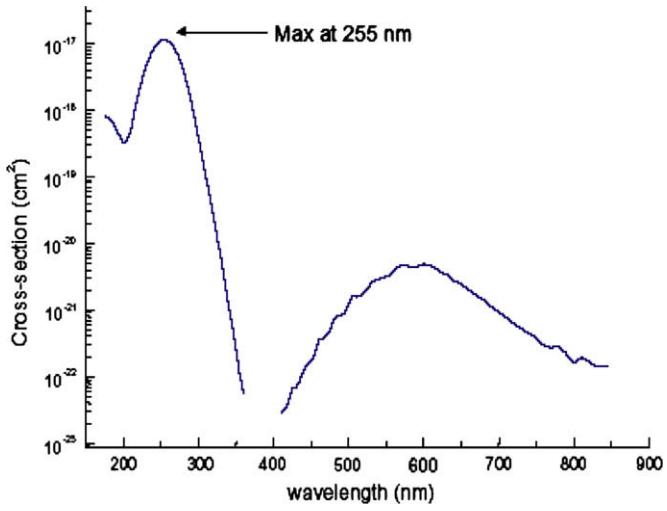

Fig. 6. Wavelength dependence of ozone absorption cross-section (Molina and Molina, 1986).

background noise. It is defined as the ratio of the total received power to noise power signal due to the fluctuation, background light or electrical noise and is given by (Demtröder, 2003):

$$\mathrm{SNR} = \frac{P_s(\lambda_{on}, R)}{\mathrm{NEP}} = P_s(\lambda_{on}, R)\frac{D^*}{\sqrt{A_d \Delta f}} \tag{13}$$

where A_d is the sensitive area of detector, Δf is the frequency bandwidth of detector/amplifier, P_s is the lidar signal power incident on the detector and $D^* = D\sqrt{A_d \Delta f}$ [cm $\mathrm{Hz}^{1/2}$ W^{-1}] denotes normalized detectivity of the detector, where $D = 1/\mathrm{NEP}$ is detectivity and NEP represents noise equivalent power. A greater SNR indicates the higher signal over background noise.

On the other hand, the maximum range of detection is corresponding to the lowest acceptable SNR. Usually an SNR of 1.5 is commonly considered as the lower detection limit of an accurate detector. Hence, from Eq. (13), the minimum detectable power is written as below:

$$P_{s,\min}(\lambda_{on}, R) = 1.5 \times \mathrm{NEP} \tag{14}$$

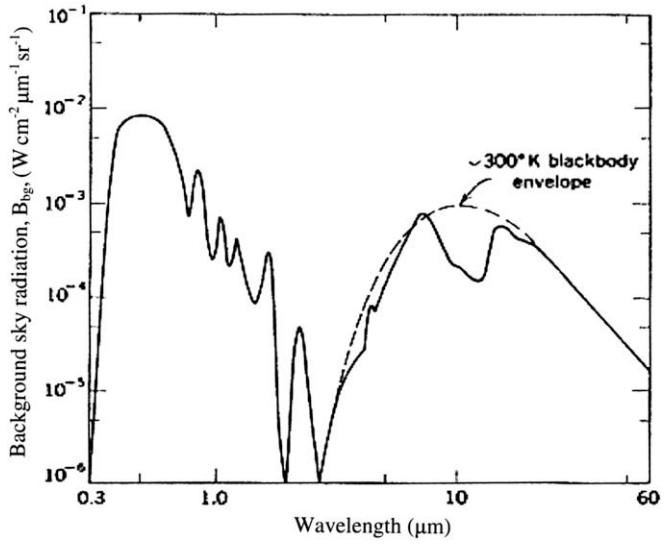

Fig. 7. Background spectral radiance distribution, B_{bg}, of the cloudless sky (Partt, 1969).

Typically, for a photomultiplier tube sensitive in UV region having dark current of 0.5 nA, resposivity of ~0.05 A/W and 1 ns rise time, the minimum detectable power is determined to be $\sim 2 \times 10^{-8}$ W at $\lambda_{on} = 351.46107$ nm. It indicates, according to Eq. (5), that the identification of 0.1 ppb uranium within a radioactive plume located at 100 m afar is accomplished using a UV laser having ~1 mj/pulse and 10 ns duration.

Substituting Eq. (12) into Eq. (13), the minimum detectable power at λ_{off} is given by:

$$P_{s,\min}\left(\lambda_{off}, R\right) = 1.5 \times \mathrm{NEP} \times \exp\left(2\int_0^R \Sigma(\lambda, R)\mathrm{d}R\right) \tag{15}$$

where $\Sigma(\lambda, R) = N(R)\Delta\sigma$ denotes the differential absorption coefficient. One of the advantages of this equation is its independence on the dynamic atmospheric volume backscatter coefficient, β, which is usually a varying parameter due to the unstable meteorological conditions. The laser peak power P_0 is determined by Eq. (5), subsequently.

Fig. 8 plots the lidar range in terms of the effective detectivity parameter, $P_{s,\min}(\lambda_{off}, R)(D^*/\sqrt{A\Delta f})(1/1.5)$, to determine the maximum detectable range as a function of $P_s(\lambda_{off},R)$ for several plume differential absorption coefficients. It can be seen, when the sensitivity of PMT increases or the laser power scales up, it increases nonlinearly. Similarly, it strongly depends on the concentration and the cross-section of the plume components.

Fig. 9 illustrates the peak power of laser probes versus uranium absorption coefficient and the corresponding uranium concentration in UV and visible spectrum (351.46107 and 591.5385 nm) for various ranges of detection.

We conclude that DIAL can be exploited for the real time radioactive plume monitoring, in emergency condition as well as the normal operation of nuclear power plant. However, the concentration of the effluents increases to become noticeable above the background level when an accident, such as loss of coolant accident (LOCA), occurs. Power excursion accident is categorized as the other major accident in the reactor vessel (Lamarsh, 1983; Glasstone and Sesonske, 1994; United Nations Scientific Committee on the Effects of Atomic Radiation, 1988).

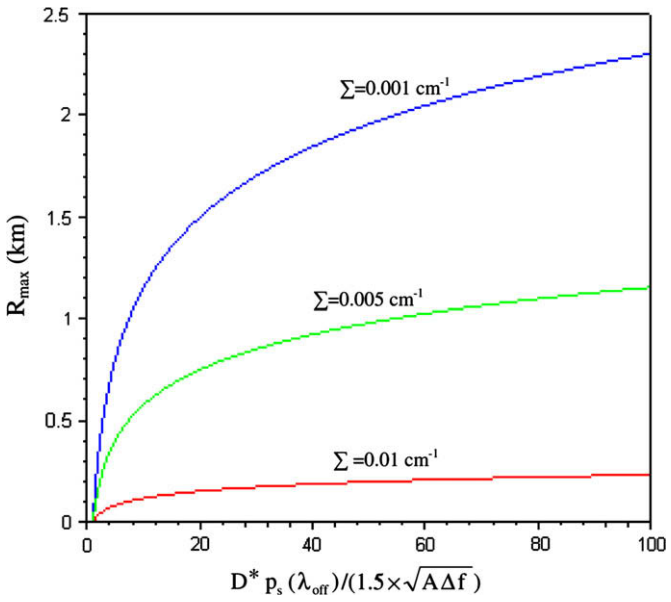

Fig. 8. DIAL maximum range detection versus PMT characteristic parameter, $P_{s,\min}(\lambda_{off}, R)(D^*/\sqrt{A\Delta f})(1/1.5)$, for various differential absorption coefficients $\sum = N[\sigma_{abs}(\lambda_{on}) - \sigma_{abs}(\lambda_{off})]$.

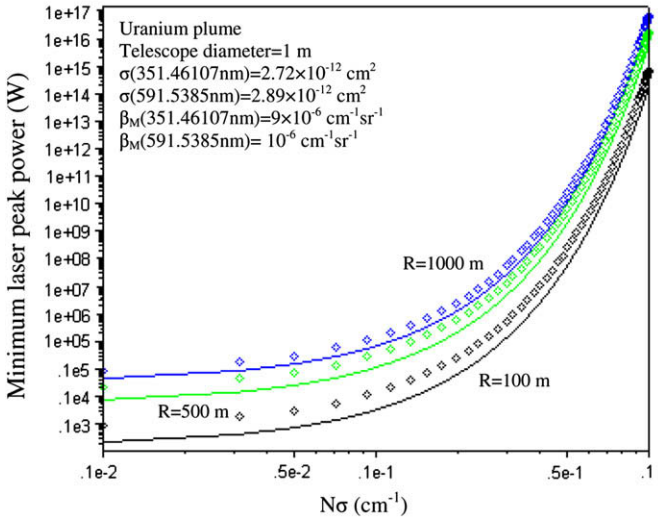

Fig. 9. Minimum laser peak power versus absorption coefficient, $N\sigma$, in order to detect the released uranium into the atmosphere. Solid line and dashed line represent $\lambda_{on} = 351.46107$ and 591.5385 nm, respectively.

Based on the definition of activity, the radionuclide density, N, containing a certain isotope of a sole radioactive element is given by:

$$N = Ct_{1/2}/\ln(2) \tag{16}$$

where C (Bq/m^3) and $t_{1/2}$ are the specific activity and the corresponding half-life of the species, respectively.

Practically, N is determined by DIAL using the logarithmic derivative of the backscattered signals at λ_{on} and λ_{off} . Combining Eqs. (2), (12) and (16), the Nuclear-DIAL equation is derived as below

$$\frac{4\pi MR^2 t_{1/2}}{AT_{int}}\exp(\mu R) = \frac{\ln(2)}{2\Delta\sigma}\frac{d}{dR}\left(\ln\frac{P_s(\lambda_{off},R)}{P_s(\lambda_{on},R)}\right) \tag{17}$$

Fig. 10 depicts phoswich characteristic parameter ($4\pi Mt_{1/2}/AT_{int}t$) in terms of species concentration, N, based on Eq. (12). It demonstrates the characteristic graph for the hybrid system performance. It explains that the function of phoswich improves

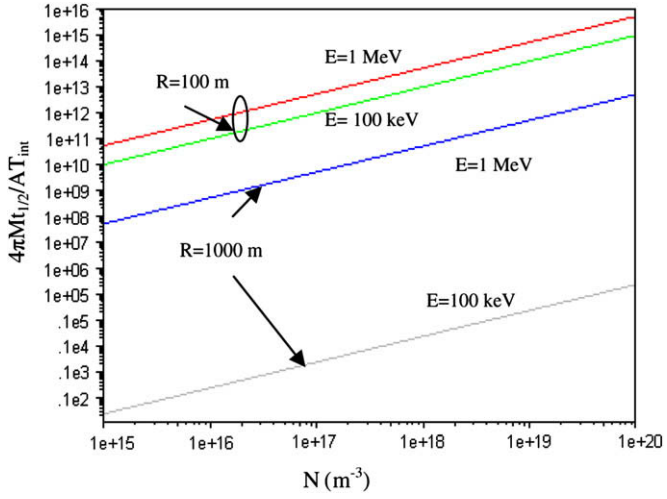

Fig. 10. Phoswich characteristic parameter in hybrid system, $4\pi Mt_{1/2}/AT_{int}$, versus plume concentration at various X/γ energies for different plume locations R.

efficiently in the hybrid system such that: (i) the phoswich count, M, is linearly proportional to the species concentration, N; and (ii) the hybrid system energy resolution becomes much better than phoswich at longer ranges.

2.3. Broadband tunable UV laser

In atomic absorption remote sensing, a laser should be reliable and possesses characteristics such as wide wavelength tuning range from the visible to the deep UV, narrow spectral linewidth, high repetition rate, compactness, and a relatively low price. Various coherent sources, such as dye, diode and Ti:Al_2O_3 lasers as well as the optical parametric oscillator (OPO) have been employed. Among those lasers, OPO does not fit wide application in high resolution atomic spectroscopy mostly due to the lack of frequency and linewidth stability in order of atomic linewidth ~0.01 cm^{-1}. In addition, the excimer and the higher harmonic Nd:YAG lasers are taken into account as the alternatives to monitor some of radionuclides. For long-range remote sensing, the multistage amplifiers of dye or Ti:Al_2O_3 lasers can be exploited to scale up the pulse energy of the laser probe.

Broadband dye and Ti:Al_2O_3 gain media are often desirable to tune a specific wavelength over the bandwidth without changing the cavity mirrors. The dye laser pumped by SHG of Nd:YAG laser offers a wide tunability mainly by changing the dye solutions such as Coumarine and Rhodamine with the spectral emission at 400–500 nm and 570–610 nm, respectively. The higher harmonic of those lasers cover the spectral range of 200–400 nm. The Ti:Al_2O_3 laser, pumped by a frequency stable SHG Nd:YAG laser at 532 nm, is mostly used as a tunable NIR laser with very broad emission bandwidth 660–1180 nm to generate ns short pulses. The higher harmonic generations of those lasers lie within the attractive UV spectrum of the atomic absorption. The most conventional lasers for remote sensing are recommended in Tables 1 and 2.

For instance, the corresponding UV absorption lines (λ_{on}) of ^{238}U are 351.46107, 356.18038, and 358.48774 nm, which lie on the SHG spectrum of Ti:Al_2O_3 laser. Similarly, the remote sensing of ^{230}Th is performed at 371.94347 nm using SHG of that laser and ^{234}Pa from uranium chain may be traced at the corresponding absorptive lines of 398.223. XeF laser at 351 nm is also the other choice for uranium remote sensing.

During emergency conditions of an operating reactor, the leakage of Samarium drastically increases due to LOCA. The strong samarium absorption line at 463.2320 nm can be matched well with the fundamental harmonic of coumarine laser as well.

It is understood that the narrow linewidth of the absorption spectra of atoms is Doppler-limited which is about 0.01 cm^{-1} or about 1 pm at 300 nm with a corresponding isotope shift is in order of 0.1 cm^{-1}. In addition, the hyperfine structure due to the presence of nuclear spin is much smaller than the splitting caused by electron spin. Various arrangements, such as Hansch array, Double-Quartet prism method and Littman setup are available to perform tuning the emission of tunable lasers. Littman setup is chosen mainly because of easy alignment to achieve single mode with spectral width as narrow as 0.01 cm^{-1}. For the additional linewidth narrowing, intracavity Fabry-Perot etalons or birefringent crystal waveplates can be utilized. The diffraction grating used in Littman arrangement operates as a beam expander and a dispersion element simultaneously, so that the dispersion power becomes two times higher than that of the Littrow mount. Fig. 11(a) and (b) shows Littman-type tunable Ti:Al_2O_3 and dye lasers using an intracavity grazing incidence grating.

As shown in Fig. 9, DIAL range in the clean atmosphere, is achievable up to several km using the oscillator–amplifier array. However, the effective range of interactive hybrid system is restricted by the phoswich performance to a few km.

Generally, the spectral emission of most lasers characterizes a bandwidth of 0.1–1 cm^{-1}. Even though the isotopes of a radionuclide possess the isotope shift less than 1 cm^{-1}, the selective detection of a desired isotope is achieved using the dispersive optics associated with single mode arrangement of the resonator to reach laser bandwidth as short as 0.01 cm^{-1} accompanying by the temperature and frequency stabilization. Alternatively, in order to avoid the implementation of DIAL with such a high spectral resolution, phoswich is employed to identify the relative X/γ emissions of the different isotopes. It is taken into account as a figure of merit for the hybrid system to prevent using sophisticated laser systems. If the aim is not the isotopic identification of radionuclide, then a broadband laser can be employed effectively where the laser bandwidth is chosen to be in order of the adjacent absorptive lines of the radionuclides.

3. External dose rate

A unique application of hybrid system is to determine external dose rate. Radiation dose received from the airborne radioactive material that might escape from the reactor containment is assumed to be similar to that from a smokestack but closer to the ground. The plume moves in x-direction by the wind while it diffuses in two perpendicular directions, i.e. laterally (or cross wind) and vertically as shown in Fig. 12. Observation made on small plume indicates that the diffusion acts as a Gaussian distribution of the plume about a centerline. According to the Gaussian plume model, presuming that the containment constitute a continuous point source, then the radioactivity distribution of a specific radionuclide on the ground, would be represented by (Lamarsh, 1983; Glasstone and Sesonske, 1994):

$$\chi(x,y,h) = \frac{Q}{\pi v_x \sigma_y \sigma_z} \exp\left(-\frac{1}{2}\left(\frac{h^2}{\sigma_z} + \frac{y^2}{\sigma_y}\right)\right) \quad (18)$$

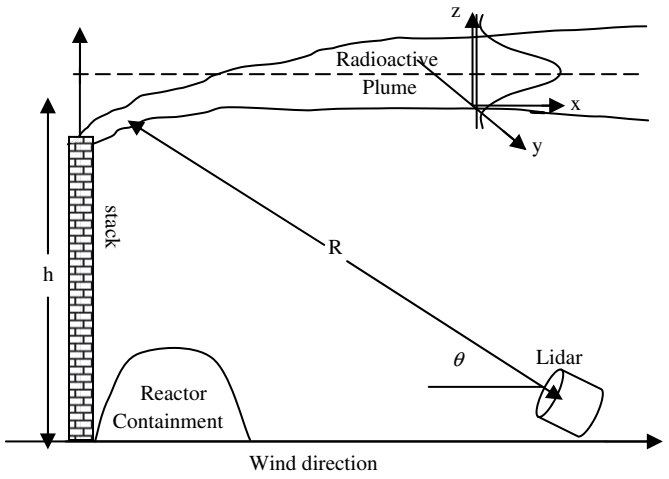

Fig. 12. Simplified geometry of monitoring released radioactive materials above the stack of a nuclear power reactor by DIAL system.

where volume activity, χ, (Ci/m^3) is the concentration of radioactivity at a point (x, y) on the ground; Q (Ci/s) is the rate of released activity at top of the stack which is determined by the hybrid system. Moreover, v_x (m/s) denotes the wind speed in the x-direction, h (m) is the effective height of the radioactivity release (here, height of reactor stack), and y (m) ascertains the lateral distance of the detector from the plume centerline; σ_y and σ_z are defined to be the standard deviations of the plume distribution in y (lateral) and z (vertical) directions, respectively.

Those depend on both atmospheric stability and the distance from the source. Experimental data shows that σ_y and σ_z increase as $x^{1/0.894}$ from the point of emission. Pasquill obtained a set of curves for σ_y and σ_z at six different atmospheric stability conditions, such

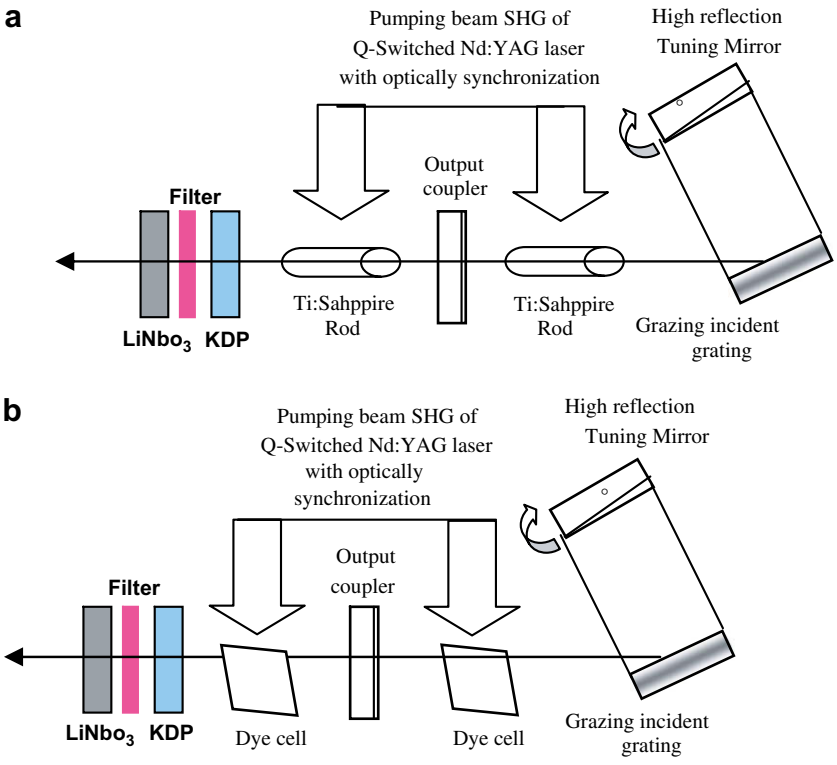

Fig. 11. Schematic tunable UV oscillator-amplifier of (a) Littman-type Ti:Al_2O_3 laser, (b) Littman-type dye laser (Parvin et al., 2003).

that less stable conditions have the higher values of both σ_y and σ_z than stable one (Vesilind et al., 1988).

The value of χ is largest along the centerline of the plume, where $y = 0$. The concentration is rewritten as below:

$$\chi(x,h) = \frac{Q}{\pi v_x \sigma_y \sigma_z} \exp\left(-\frac{h^2}{2\sigma_z}\right) \tag{19}$$

It is noticeable to emphasize that v_x and h of the plume are determined by DIAL response based on the geometry of detection and the time of flight (TOF) measurements.

The external equivalent dose rate $\dot{H}$ (rem/s) from an infinite uniform plume located above ground level, containing a single radionuclide at a concentration of χ (Ci/m^3), with the quality factor equivalent to unity for a single gamma energy, E_γ (MeV), is written approximately as below:

$$\dot{H} = 0.262 \overline{E}_{\gamma,x} \chi \tag{20}$$

Substituting χ from Eq. (15) into Eq. (16) we find:

$$\dot{H} = \frac{0.262 \overline{E}_{\gamma,x} Q}{\pi v_x \sigma_y \sigma_z} \exp\left(-\frac{h^2}{2\sigma_z}\right) \tag{21}$$

Thus, equivalent dose rate is calculated by data acquisition from the phoswich to identify corresponding γ energies of the photopeaks as well as the determination of the plume range and the species concentration from the DIAL. For several types of radionuclides within the plume, Eq. (15) should be a summation over all γ energies, such that, $\overline{E}_\gamma$ attributes to the average energy of the all gamma rays.

Fig. 13 is the graphical representation of Eq. (21). It shows the quantity $v_x \dot{H}/E_\gamma Q$ for the effluent released above the reactor stack versus distance x afar. It represents that maximum $\dot{H}$ occurs at a certain distance $x = (h/\sqrt{2})^{0.894}$. It arises from the fact that the plume diffuses vertically downward to reach the ground level.

Furthermore, in order to estimate the external dose rate, volumetric activity, χ, is determined from Eq. (19) while, the rate of release of activity above the stack, Q, is obtained from Fig. 10 corresponding to Eq. (17).

Tables 1 and 2 give values of E_γ for the most important gaseous fission products emanated from the reactor vessel. Those are released into the environment in small quantities during the normal operation of a reactor to become a significant amount during an accident.

4. Result and discussion

Radioactive pollutants which are released from the waste or the probable explosion of nuclear site during the accident are known to be extremely hazardous for human health, therefore those must be quickly identified and well protected. Here, a new method is investigated for remote sensing of an unknown radioactive plume having gamma or X emitter radionuclides including uranium chain or transuranium elements to help ensure that nuclear power plants operate safely to be non-deterimental to human and environmental well-being. Hybrid system can be used for continuous, atmospheric mapping and systematic monitoring of radioactive plume constituents based on the optical remote sensing DIAL and phoswich detector arrangements.

In a reactor accident, the radionuclides such as fission products are first released into the containment building and subsequently may leak to the atmosphere. The activity of the resulting effluent depends on the rate at which this leakage occurs. In addition to the released gaseous products such as I, Xe, Kr and Sm which easily escape the nuclear power plant containment, the other radionuclides, such as U and Pu can also be released, because of the fuel evaporation due to high temperature.

In general, interaction of laser with plume released above the stack at reactor normal operation could be Rayleigh scattering. However, the concentration of the effluents increases to become noticeable above background level when an accident such as LOCA occurs. Power excursion is categorized as another major accident in the reactors, when steam explosion of the pressure vessel leads to the release of heavy plume including various nuclides with a dense cloud to such an extent that Mie scattering becomes dominant. The tuned laser probe can be used for the prompt identification and quantification of the accidental radioactive leakage to the atmosphere as well as normally radionuclide release in ppb (or less) around the stacks of nuclear power plant or radioisotope labs, reprocessing plant and the conversion facilities.

The interactive performance of the hybrid system is shown in Fig. 14. The arrangement includes two main sections of phoswich detector array and DIAL system which interact with each other through a processor unit to operate simultaneously. Field of view of

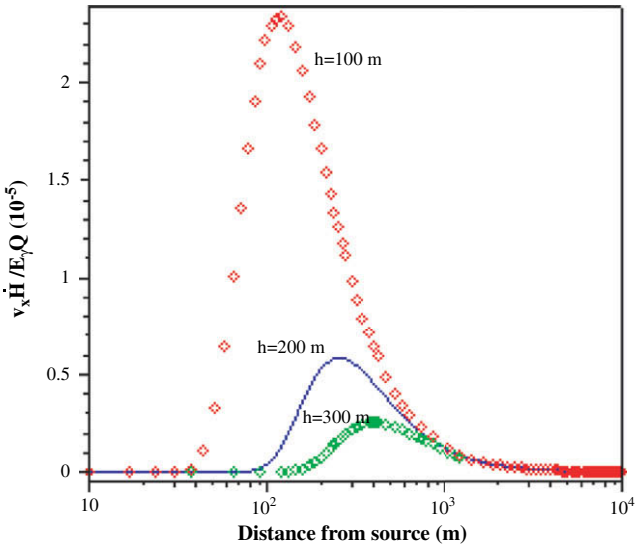

Fig. 13. External dose rate equivalent parameter, $v_x \dot{H}/E_\gamma Q$, versus distance from reactor stack.

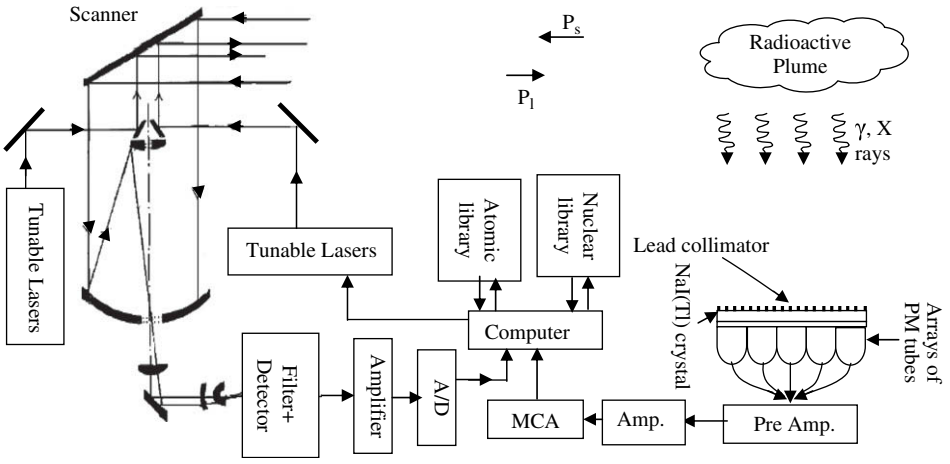

Fig. 14. Performance of phoswich–DIAL hybrid system.

phoswich array is aligned to the top of the reactor stack to determine the radioactive plume. The processor unit commands to phoswich detector array to integrate the signal in the definite time interval along plume direction. The process carries out by detecting γ/X-ray photopeaks, using nuclear library, then the radionuclide species and their half-life can be determined. If there is more than one radionuclide, those can be identified by searching photopeak energies on MCA. In the stage of X/γ detection, using phoswich, the photopeaks of the characteristic hard X-ray of transuranium (30–300 keV) elements can be identified, if available within the radioactive plume. For instance, the typical photopeaks of ^{241}Am, ^{239}Pu and ^{235}U denote to be 59.5, 38.7 and 11.5 keV, respectively.

On the other hand, high energetic photons due to the γ emitter radionuclides may generate light in both scintillators accordingly. For example, the well known γ emitter ^{137}Cs with photon energy 661.6 keV having 852.113 nm absorption line can be detected by a tunable fundamental Ti:Saphire laser. If there are simultaneous signals from electronic discriminators, it will identify the γ source species, using the nuclear library data. Similarly, if the discriminator distinguishes a single signal from NaI detector, then the X-ray library is used to determine the transuranuim elements. Those photopeaks do not discern the plume location by themselves. It may be an X/γ-ray emitted from a far field dense plume or a near field dilutes one. Therefore, it is necessary to quantify the species by a differential absorption lidar. When the radioactive species were identified, the processor searches absorption lines through atomic library data and commands to DIAL unit to tune laser line at λ_{on} and send a pulse to the atmosphere. DIAL tunes the tunable lasers such as Ti:Saphire or dye laser on the typical absorption lines of the identified elements to determine the relative concentration and external dose rate of the species using the logarithmic derivatives of the backscattered signal at λ_{on} and λ_{off} (Glasstone and Sesonske, 1994). The backscattered photons are received by a Cosegarian telescope conducted through a bandpass filter to a sensitive PMT. The telescope diameter is chosen to be the same as that of phoswich which encircles ∼80 phoswich having ∼100 cm^2 area. The intensity of the backscattered light can be recorded as a function of time. In the mean while, TOF is measured to determine the plume distance and the velocity of the plume.

Here we intend to identify uranium within the plume. XeF broadband laser with ∼1 nm linewidth covers the uranium absorption line at 351.4610 nm for the long-range remote sensing while SHG Ti:Saphire laser is an alternative source.

Range, concentration, volumetric activity χ, and photon energy E_γ, are identified and the external dose rate $\dot{H}$ can be determined based on Eq. (21), subsequently. The universal graphs are used to predict the functions of the hybrid system.

The relative activity and the type of radionuclide are identified by phoswich and similarly $t_{1/2}$ can be extracted from nuclear library data, while λ_{on} is determined via atomic library, to tune at strongest absorption transition, in order to evaluate the absolute concentration of the radionuclide.

Here uranium element is chosen to show the capability of the hybrid system to measure the remote radionuclides as well as the external dose rate. Using Eq. (10), UV absorption cross-sections of the nuclide at 351.46107 nm was determined to be 2.7×10^{-12} cm^2. For the remote sensing of uranium element at $\lambda_{on} = 351.46107$ nm (or $\lambda_{on} = 591.5385$ nm), $T_{O_3}(R)$ was estimated to be $\sim 10^6$ cm^{-3} (or $\sim 10^3$ cm^{-3}). Comparatively, the noise concentration caused by ozone is noticeably small as it is negligible during uranium sensing above the stack of the fuel fabrication facilities ∼0.01–0.1 ppb (United Nations Scientific Committee on the Effects of Atomic Radiation, 1988).

On the other hand, the absorption spectrum of the major uranium isotope ^{238}U at 591.5385 nm and the corresponding hyperfine structure of ^{235}U are shown in Fig. 15. It deduces that ^{235}U owns eight major separate peaks denoting A, B, …, H corresponding to $\Delta F = +1$ transitions and the seven minor separate peaks a, b, …, f due to $\Delta F = 0$ transitions. However, the transition related to $\Delta F = -1$ could not be detectable. In general, 15 peaks are distinguished as the hyperfine structure of ^{235}U. It is obvious that ^{238}U with even number of nucleus does not show such behavior because of zero nuclear spin. Typically, the isotopes shift of uranium at 591.538 nm is ∼0.3 cm^{-1} (or 0.01 nm) which represents one order of magnitude higher than that of Doppler broadening (Böhm et al., 1978).

It also indicates that the level splitting of ^{235}U is ∼0.05 cm^{-1}. If laser linewidth is chosen to be equivalent to Doppler-limited linewidth of the target, then both isotopes of (^{238}U and ^{235}U) can be distinguishably detected. However, the natural uranium contains ^{238}U with the abundance of 99.3%, adequate to tune at the major isotope absorption line. Despite, the power reactor's fuel is usually enriched up to few percent, however the major isotope is known to be ^{238}U.

Eventually, we have correlated available theoretical and experimental data for uranium remote sensing. The uranium cross-section from Eq. (10), experimental absorption spectrum around 591.5385 nm (Fig. 15) as well as the theoretical backscatter coefficient, β_M from Eq. (7), and the experimental ozone absorption spectrum, Fig. 6, and the corresponding cross-section and nominal

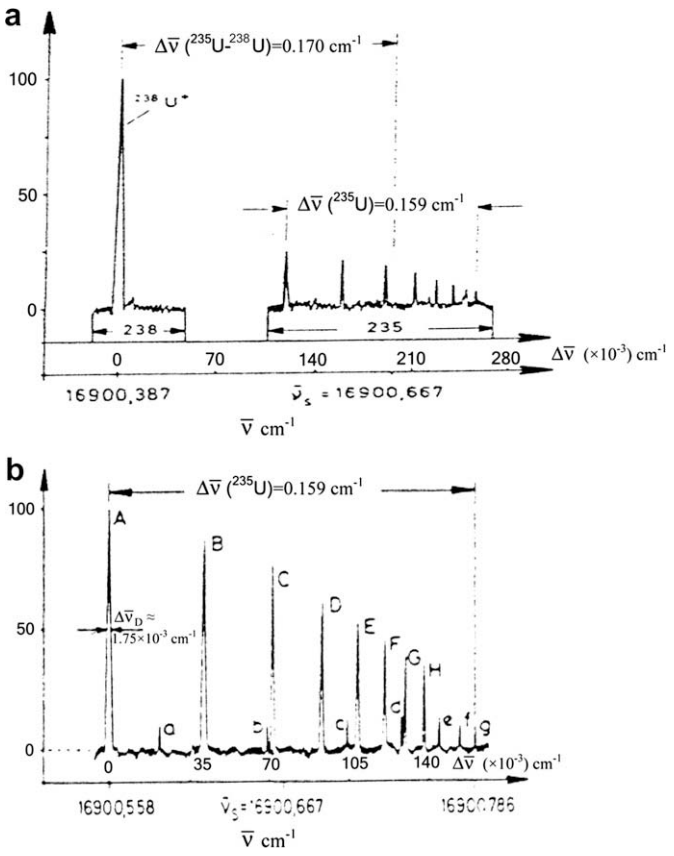

Fig. 15. Absorption spectrum of ^{235}U and ^{238}U at 591.5385 nm (a), and hyperfine structure of ^{235}U (b) (Böhm et al., 1978).

O_3 concentration (~0.01 ppm) are used to determine the minimum peak power of laser probe as depicted in Fig. 9.

5. Conclusion

In this work, the feasibility of hybrid system to sense a remote uranium plume was investigated, using the uranium absorption spectrum with hyperfine structure, the corresponding absorption cross-section based on Eq. (10) as well as the nominal concentrations above the stack in the normal and accidental conditions.

Moreover, the serious incapability of phoswich for pointing and identification of an unknown radioactive plume in the atmosphere, as depicted in Fig. 5, has been strongly improved using DIAL–phoswich combination according to nuclear-lidar Eq. (17), and the graphical representation as shown in Fig. 10. The hybrid system functions as an interactive process including a slow response, time integrated phoswich array and a fast, real time DIAL as illustrated in Fig. 14.

A certain phoswich counting, at a chosen integration time, may be due to a high active source with low γ energy emission or oppositely a dilute radioactive plume emitting high energy photons. Moreover, it may be due to a dense plume afar or a weak effluent nearby for the identical X/γ energy emissions according to Fig. 5. Alternatively, the hybrid system exhibits a linear correlation between the counts and the concentration of the species. It indicates a unique counting corresponding to a certain activity owning the potential to resolve X/γ energies effectively at longer ranges as shown in Fig. 9. Finally, despite phoswich is unable to determine the external dose, however, the hybrid system does.

Acknowledgements

The authors would like to thank Professor Pier Benetti from the University of Pavia (Italy) and member of the Italian Nuclear Physics Institute, INFN, for his fruitful comments particularly on phoswich detection.

References

Axner, O., Gustafsson, J., Omenetto, N., Winefordner, J.D., 2004. Line strengths, A-factors and absorption cross-section for line structure lines in multiples and hyperfine structure components in lines in atomic spectroscopy– a user's guide. Spectrochemica Acta Part B 59, 1–39.

Böhm, H.D.V., Michaelis, W., Weitkamp, C., 1978. Hyperfine structure and isotope shift measurements on ^{235}U and laser separation of uranium isotopes by two-step photoionization. Optics Communications 26 (2).

Beniston, M., Wolf, J.P., Beniston-Rebertz, M., Kolsch, H.J., Rairoux, P., Woste, L., 1990. Use of lidar measurements and numerical model in air pollution research. Journal of Geophysical Research 95, 9879–9894.

Camagani, P., Sandroni, S. (Eds.), 1984. Optical Remote Sensing of the Air Pollution. Elsevier Science Publisher, B V, pp. 123–150.

Chistrykova, L.K., Kopytin, Y.D., 2005. Spectroradiometric inspection of nuclear pottution in the atmosphere based on photochemical effects. Optical Engineering 44, 71,210–71,223.

Demtröder, W., 2003. Laser Spectroscopy: Basic Concepts and Instrumentation, third ed. Springer.

Derava, P., Raj, P.E., Padithurai, G., Dani, K.K., Sonbawne, S.M., Excimer-Raman DIAL probing of atmospheric ozone over an urban station: first result. In: Proceedings of 22nd International Laser Radar Conference, Italy, Matara.

Drake, G.W.F. (Ed.), 2006. Springer Handbook of Atomic, Molecular and Optical Physics. Springer Science+Business Media Inc..

Edner, H., Fredriksoon, K., Sunesson, A., Svanberg, S., Uneus, L., Wendt, W., 1987. Mobile remote sensing system for atmospheric monitoring. Applied Optics 26, 4330–4338.

Egeback, A., Fredriksson, K., Hertz, H., 1984. DIAL techniques for the control of sulfur dioxide emission. Applied Optics 23, 722–729.

Farsoni, A.T., Hamby, D.M., 2007. A system for simultaneous beta and gamma spectroscopy. Nuclear Instruments and Methods in Physics Research Section A 578, 528–536.

Fredriksson, K., Galle, B., Nytrom, K., Svanberg, S., 1979. Lidar system applied in atmospheric pollution monitoring. Applied Optics 18, 2998–3003.

Frontera, F., Costa, E., Dal Fiume, D., Feroci, M., Nicastro, L., Orlandini, M., Palazzi, E., Zavattini, G., 1997. The high energy instrument PDS on-board the BeppoSAX X-ray astronomy satellite. Astronomy & Astrophysics. Supplement Series 122, 357–369.

Fugii, T., Fukuchi, T., Goto, N., Nemoto, K., Takeuchi, N., 2001. Dual differential absorption lidar for the measurement of atmospheric SO_2 of the order of parts in 10^9. Applied Optics 40, 949–956.

Fujii, T., Fukuahi, T., 2005. Laser Remote Sensing. Taylor & Francis Group.

Garroway, A.N., Buess, M.L., Miller, J.B., Suits, B.H., Hibbs, A.D., Barrall, G.A., Matthews, R., Burnett, L.J., 2001. Remote sensing by nuclear quadrupole resonance. IEEE Transactions on Geosciences and Remote Sensing 39, 1108–1118.

Glasstone, S., Sesonske, A., 1994. Nuclear Reactor Engineering. Chapman & Hall, Inc., New York.

Guerra, D.V., Coyle, D.B., Krebs, D.J., 1994. A completely solid state Ti:sapphire laser system for lidar and atmospheric spectroscopy. Measurement Science and Technology 5, 1306–1308.

Hannon S.M., Gatt P., Henderson S.W., June 23–27, 1997. Continental U.S. aerosol backscatter at 2 μm: distribution and implications for ground-and space-based coherent lidars. In: Proceedings of the 9th Conference on Coherent Laser Radar, 176, Linkoping, Sweden.
<http://atom.kaeri.re.kr/ton/>.

Kildal, H., Byer, R.L., 1971. Comparison of laser methods for the remote detection of atmospheric pollutants. In: Proceedings of IEEE Conference. Institute of Electrical and Electronics Engineers, New York, pp. 1644–1663.

Knoll, G.F., 2000. Radiation Detection and Measurement, third ed. Wiley, New York.

Kobayashi, T., Imaki, M., Takegoshi, Y., Sugimoto, N., 2004. UV high-spectral-resolution lidar for absolute measurement of aerosol extinction coefficient and lidar-ratio. In: Proceedings of 22nd International Laser Radar Conference, Italy, Matara.

Lamarsh, J.R., 1983. Introduction to Nuclear Engineering. Addison Wesley.

McKay, J.A., 1999. Single and tandem Fabry-Perot etalons as solar background filters for lidar. Applied Optics 38, 5851–5858.

Molina, L.T., Molina, M.J., 1986. Absolute absorption cross-sections of ozone in the 185- to 350-nm wavelength range. Journal of Geophysical Research 91 (D13), 14,501–14,508.

Nakazato, M., Nagai, T., Sakai, T., Kabayashi, T., 2006. Case study of urban air pollution over Taukauba as observed by UV ozone DIAL. In: Proceedings of 23rd International Laser Radar Conference, Japan, Nara.

National Institute of Technology, Gaithersburg, MD, USA, NIST Atomic Spectra Database. Available from: <http://physics.nist.gov/PhysRefData/Handbook/Tables/>.

Partt, W.K., 1969. Laser Communication Systems. Wiley, New York.
Parvin P., Davoudabadi Gh.R., 2007. Iranian patent registration no: 32585, registration date: Sept. 06, 2005, application no: 38405162, date: Aug. 03, 2005 and US patent registration, application no: 11782647.
Parvin, P., Eslami, A., Amiri, N., 2003. Design and construction of a narrowband dye (Rd6G) laser pumped with a KrF (248 nm) laser (Littman setup) for determining the saturation intensity (I_s) and small-signal gain (γ_0) of the amplifying medium. Atmospheric and Oceanic Optics 16, 863–865.
Parvin, P., Davoudabadi, G.R., Kariminezhad, H., Zamanipour, Z., 2004. The remote-sensing of radioactive plume with a hybrid system including gamma spectroscopy and DIAL lidar. In: Proceedings of 22nd International Laser Radar Conference, Italy, Matara, pp. 291–294.
Parvin, P., Davoudabadi, G.R., Zamanipour, Z., Zangeneh, H.R., Jaleh, B., 2005. Remote element tracing of trans-uranium plumes using a interactive UV laser DIAL coupled with a phoswich detector. In: Proceedings of CLEO/Europe-EQEC, Germany, Munich.
Sood, D.D., Reddy, A.V.R., Ramamoorthy, N., 2000. Fundamentals of Radiochemistry. IANCAS.
Svanberg, S., 2001. Atomic and Molecular Spectroscopy, Basic Aspects and Practical Applications. Springer.
Uchino, O., 2006. On some lidar developments for atmospheric research. In: Proceedings of 23rd International Laser Radar Conference, Japan, Nara.
United Nations Scientific Committee on the Effects of Atomic Radiation, 1988. Report to the General Assembly, with Annexes, Sources, Effects and Risks of Ionizing Radiation. United Nations Publication, New York.
Vaughan, J.M., 2002. Scattering in the atmosphere. In: Pike, E.R., Sabatier, P.C. (Eds.), Scattering- Scattering and Inverse Scattering in Pure and Applied Science. Academic Press, San Diego, CA.
Vesilind, P.A., Peirce, J.J., Weiner, R., 1988. Environmental Engineering, second ed. Publishing (U.S.A.)Inc.
Weitkamp, C. (Ed.), 2005. Lidar: Range-Resolved Optical Remote Sensing of the Atmosphere. John Wiley & Sons, New York.